Research Article

For reprint orders, please contact: reprints@futuremedicine.com

Nanomedicine

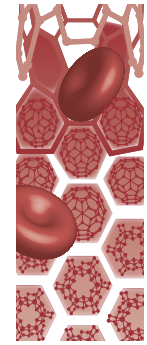

Bone-targeted cabazitaxel nanoparticles for metastatic prostate cancer skeletal lesions and pain

Aim: The aim of this study was to develop a novel cabazitaxel bone targeted nanoparticle (NP) system for improved drug delivery to the bone microenvironment. **Materials & methods:** Nanoparticles were developed using poly(D,L-lactic-co-glycolic acid) and cabazitaxel as the core with amino-bisphosphonate surface conjugation. Optimization of nanoparticle physiochemical properties, *in vitro* evaluation in prostate cancer cell lines and *in vivo* testing in an intraosseous model of metastatic prostate cancer was performed. **Results:** This bone targeted cabazitaxel nanocarrier system showed significant reduction in tumor burden, while at the same time maintaining bone structure integrity and reducing pain in the mouse tumor limb. **Conclusion:** This bone microenvironment targeted nanoparticle system and clinically relevant approach of evaluation represents a promising advancement for treating bone metastatic cancer.

Andrew S Gdowski[1], Amalendu Ranjan*[,1], Marjana R Sarker[2] & Jamboor K Vishwanatha[1]

[1]Institute for Molecular Medicine, University of North Texas Health Science Center, 3500 Camp Bowie Blvd, Fort Worth, TX 76107, USA

[2]Center for Neuroscience Discovery, University of North Texas Health Science Center, 3500 Camp Bowie Blvd, Fort Worth, TX 76107, USA

*Author for correspondence:
Tel.: +1 817 735 2138
amalendu.ranjan@unthsc.edu

First draft submitted: 23 May 2017; Accepted for publication: 18 July 2017; Published online: 14 August 2017

Keywords: bone metastasis • cabazitaxel • polymeric nanoparticle • prostate cancer • targeted therapeutic

Despite improved overall survival in cancer patients over the past 50 years, limited advances have been made in treating patients with metastatic cancer. Various types of cancer metastasize to specific locations in the body. Among these, prostate cancer exhibits increased capacity to create bone specific lesions with high frequency [1]. Once bone localization takes place, treatment regimens are inadequate and overall survival is poor [2]. Nearly all patients who die from prostate cancer will have skeletal involvement [1]. These bone metastases often cause debilitating and life threatening problems including: uncontrollable pain, hypercalcemia, broken bones, spinal cord compression and the inability to perform activities of daily living.

Several barriers exist to developing optimal therapy for bone metastatic prostate cancer. At the molecular level, receptor activator for nuclear factor κB (RANK), its ligand (RANKL), osteoprotegerin and other signaling molecules are secreted by osteoclasts, osteoblasts and cancer cells. This creates a vicious cycle of bone turnover and increased proliferation of cancer cells [3]. Some therapeutic strategies direct treatment at the bone with drugs such as denosumab or bisphosphonates. These are effective at delaying the time to fractures and providing improvement in pain [4,5]. Other treatments for bone metastatic prostate cancer utilize androgen deprivation or cytotoxic agents [6,7]. These are effective to a point. However, prostate cancer cells will inevitably become resistant to androgen deprivation and cytotoxic agents have known toxicities which limit administration. Another strategy involves targeting bone metastasis with alpha particles using radium-223. This provides some improved overall survival [8] but may have logistical and shelf life limitations [9].

Future Medicine part of fsg

One of the current discussions revolving around optimal therapy of bone metastasis is which target or targets are most important [10]. We argue that focusing on treatment of cancer cells is most important because they are the primary insult to the system. In a previous study, we have utilized two chemotherapeutic agents, bortezomib and curcumin, which were effective in a mouse model of bone metastatic breast cancer [11].

Another challenge to effective treatment of bone metastasis is observed at the level of the tumor and the bone structure. The hydroxyapatite structure of the bone contains growth factors such as: IGF I and II, bone morphogenetic proteins, PDGF, TGF-β and FGF [12]. These factors are released as lesions develop and cause further growth and proliferation of the tumor cells. Additionally, drugs may not adequately penetrate the tumor and thus are delivered to the bone at suboptimal therapeutic levels.

Finally, *in vivo* functional assessment of clinically relevant parameters during the preclinical testing phase is often overlooked. However, there are some groups who have investigated functional assessment in the preclinical development of bone-targeted therapies for bone metastatic cancer. One recent example of a novel liposomal formulation demonstrated pain improvement in a bone metastatic model of prostate cancer after treatment with RGD peptide conjugated cisplatin liposomes [13]. Strategies like this are important because once these bone metastatic lesions have become established, severe and debilitating bone pain is a challenge to manage as performance status decreases. More research emphasis should be placed on validating pain assessment assays while testing preclinical therapies for bone metastatic cancers.

In this manuscript, we describe the engineering and validation experiments of a novel cabazitaxel encapsulated bone microenvironment targeted nanoparticle (NP) system. Bone targeting was achieved by utilizing an amino-bisphosphonate molecule attached to the surface of polymeric nanoparticles. Poly(D,L-lactic-co-glycolic acid) (PLGA) was chosen as the core of the nanoparticle for its biocompatibility and ability for controlled release of cargo. We have optimized the chemical and physical characteristics of this system and have tested the nanoformulation in both *in vitro* and *in vivo* models of metastatic prostate cancer. We have tested the efficacy in an intraosseous model of bone metastatic prostate cancer while monitoring bone structure. Finally, we have utilized behavior assays to measure pain response after treatment with the bone targeted nanoparticles.

Materials & methods

Nanoparticle formulation

The nanoparticles were prepared using a water-in-oil-in-water emulsion solvent evaporation similar to that described previously [11]. Briefly, 20 mg/ml PLGA 50:50 iv. 0.77 dl/g (~0.5% w/v in chloroform at 30°C); 124 kDa mw (Lakeshore Biomaterials) and 5% cabazitaxel (MedChem Express, NJ, USA) was dissolved in 2 ml ethyl acetate. 400 µl of phosphate-buffered saline (PBS) was added to the 2 ml ethyl acetate PLGA solution and vortexed for 30 s, followed by sonicating with ultrasonic processor UP200H system (Hielscher Ultrasonics GmbH, Germany) twice at 40% amplitude for 30 s on ice. This mixture was then transferred to an aqueous solution of 10 ml of 1% poly (vinyl-alcohol) (Sigma) plus 0.5 mg/ml of (Bis[sulfosuccinimidyl] suberate (BS3) crosslinker (ProteoChem) followed by sonication for 1 min on pulsing mode at 40% amplitude on ice. Excess solvent was evaporated under continuous magnetic stirring for 2–3 h. These nanoparticles were washed three-times by centrifugation and resuspended in water. Nanoparticles were then lyophilized on ATR FD 3.0 system (ATR Inc., MO, USA) and stored at 4°C until used.

Conjugation of alendronate on nanoparticles

Lyophilized nanoparticles and alendronate (Santa Cruz Biotechnology, CA, USA) were used at a 1:1 w/w ratio and suspended in 1 ml of PBS at room temperature for 15 min separately. Then, the two solutions were mixed together for 1 h at room temperature for alendronate conjugation. The reaction was stopped by adding 50 mM Tris Buffer (pH 7.4) for 15 min at room temperature and excess alendronate was removed by centrifugation. The nanoparticle pellet was resuspended in PBS for use.

Nanoparticle size & polydispersity index measurement

Hydrodynamic particle size and polydispersity index of targeted NP and nontargeted NP were determined by dynamic light scattering utilizing the Zetasizer Nano ZS instrument (Malvern Ltd).

Scanning electron microscopy

Surface morphology of the nanoparticles was studied using scanning electron microscopy. Lyophilized nanoparticles were imaged using a Sigma VP Field Emission Scanning Electron Microscope (Carl Zeiss Microscopy Ltd, NY, USA). Cressington 108 Auto Sputter Coater for 30 s was utilized prior to imaging. The target used for coating was gold/platinum.

Encapsulation efficiency & drug loading

The encapsulation efficiency of the cabazitaxel in the nanoparticles was determined by HPLC. First, a known amount of lyophilized nanoparticles was dissolved in

acetonitrile for 4 h. The Agilent 6460 QQQ HPLC/Mass Spectrometer system (CA, USA) equipped with a UV detector and reverse-phase C18 column (Allure C-18, 5 µm, 100 mm × 4.6 mm, Restek, Germany) with gradient mobile phase with dilutent of acetonitrile: water (1:1, v/v), mobile phase A of Trifluoroacetic acid: water (0.5:1000, v/v) and mobile phase B of Trifluoroacetic acid: acetonitrile (0.5:1000, v/v). Samples were run at a constant flow rate of 1 ml/min and the cabazitaxel quantified by integration of the area under its peak at wavelength of 220 nm and used to compare with the standard curve. The equation that was used to calculate encapsulation efficiency (EE) was: EE = (actual amount of drug encapsulated in nanoparticles)/(starting amount of drug used in nanoparticles) × 100%. Drug loading (DL) was calculated with the equation: DL = (weight of drug in nanoparticles)/(weight of nanoparticles) × 100%.

Drug release kinetics

The percentage of total cabazitaxel released at various time points was determined using a dialysis method. Nanoparticles were suspended in PBS at a concentration of 5 mg/ml. 100 µl of NP solution was added to Slide-A-Lyzer Mini Dialysis Units with 3500 MWCO (Life Technologies, CA, USA) and placed in sink conditions of 4L PBS at 37°C with stirring at 100 r.p.m. for indicated time points. At indicated time points, acetonitrile was used to recover nanoparticles and drug that remained in dialysis chamber. Amount of drug that remained in nanoparticles was quantified by HPLC as described above.

Cancer cell viability

Prostate cancer cell lines PC-3-luciferase and C4–2B-luciferase were used to assess cell viability after treatment with nanoparticles or cabazitaxel. PC-3-luciferase cells were generously provided by Dr Dan Theodorescu (University of Colorado Cancer Center) and C4–2B-luciferase cells were generously provided by Dr Even Keller (University of Michigan). PC-3 cells were grown in DMEM/F12 media supplemented with 10 mM Sodium pyruvate, 10% FBS, and 1% antibiotic-antimycotic (Gibco) while C4–2B cells were grown in RPMI-Media supplemented with 10% fetal bovine serum and 1% antibiotic-antimycotic (Gibco). Cells were plated in quadruplicate on 96-well flat bottom plates (Corning Incorporated, NC, USA) at a density of 2000 cells per well. Cells were allowed to attach for 24 h then treated with nanoparticles or free drug for a period of 24, 48 or 72 h in standard cell culture conditions. At respective time points 20 µl Tiazolyl Blue Tetrazolium Bromide (MTT) (Sigma, MO, USA) suspended in PBS at a concentration of 5 mg/ml was added to the 96-well plate. After 3 h of incubation, media were removed and 100 µl of DMSO was added to all wells and mixed by pipetting. Absorbance was read on BioTek Synergy 2 Multi-Mode Plate Reader (VT, USA) at 570 nm for triplicate samples.

3D spheroid assay

3D prostate cancer spheroid assay was used to compare cytotoxicity of nanoparticles to free drug. Cells were plated on Lipidure-Coat 96 well U bottom plate at an initial density of 1000 cells per well and cultured in standard conditions. After 48 h, spheroids were treated with nanoparticles or free drug. After 72 h of treatment, calcein AM was added to each well and fluorescent image was taken with the Olympus AX70 Florescent Microscope. Integrated fluorescent intensity of spheroids was quantified using Image J software.

Ex vivo bone binding assay

Affinity of the alendronate coated nanoparticles to the bone was determined utilizing an *ex vivo* binding assay. Accordingly, nanoparticles were formulated with Nile red dye encapsulated as a fluorescent tag and then either conjugated with alendronate on the outside or surface neutralized with Tris buffer. Freshly excised mouse femurs were cleaned of tissue and incubated in Eppendorf tubes with 5 mg/ml of nanoparticles in PBS at room temperature on gentle rocking for either 6, 24 or 72 h. At specified time points, bones were removed from nanoparticle solution, washed in PBS, and fluorescently imaged using the IVIS Animal Imaging System (Perkin Elmer, MS, USA).

Intraosseous efficacy experiment

After institutional IACUC approval, an orthotopic bone tumor model was used to test *in vivo* nanoparticle efficacy. Male athymic mice were purchased from Harlan laboratories and were 6–7 weeks old. Mice were allowed to acclimate 1 week before experiments. Mice were anesthetized with buprenorphine SR and isoflurane gas and injected at the proximal tibia with 1×10^6 PC-3 luciferase cells. Tumors developed for 1 week then randomized into groups by determining bioluminescence signal with VivoGlo Luciferin (Promega) per manufacturer's instructions so that starting bioluminescence signal was equal across treatment groups at day 7. On day 7 after tumor initiation, treatment commenced with weekly intravenous injections via lateral tail vein. Treatment groups were: saline, free cabazitaxel, nontargeted NP, and targeted NP. X-ray and bioluminescence were used to monitor groups at the final time point. At experiment termination mice were sacrificed by CO_2 asphyxiation. Lower limb tumors were removed and analyzed.

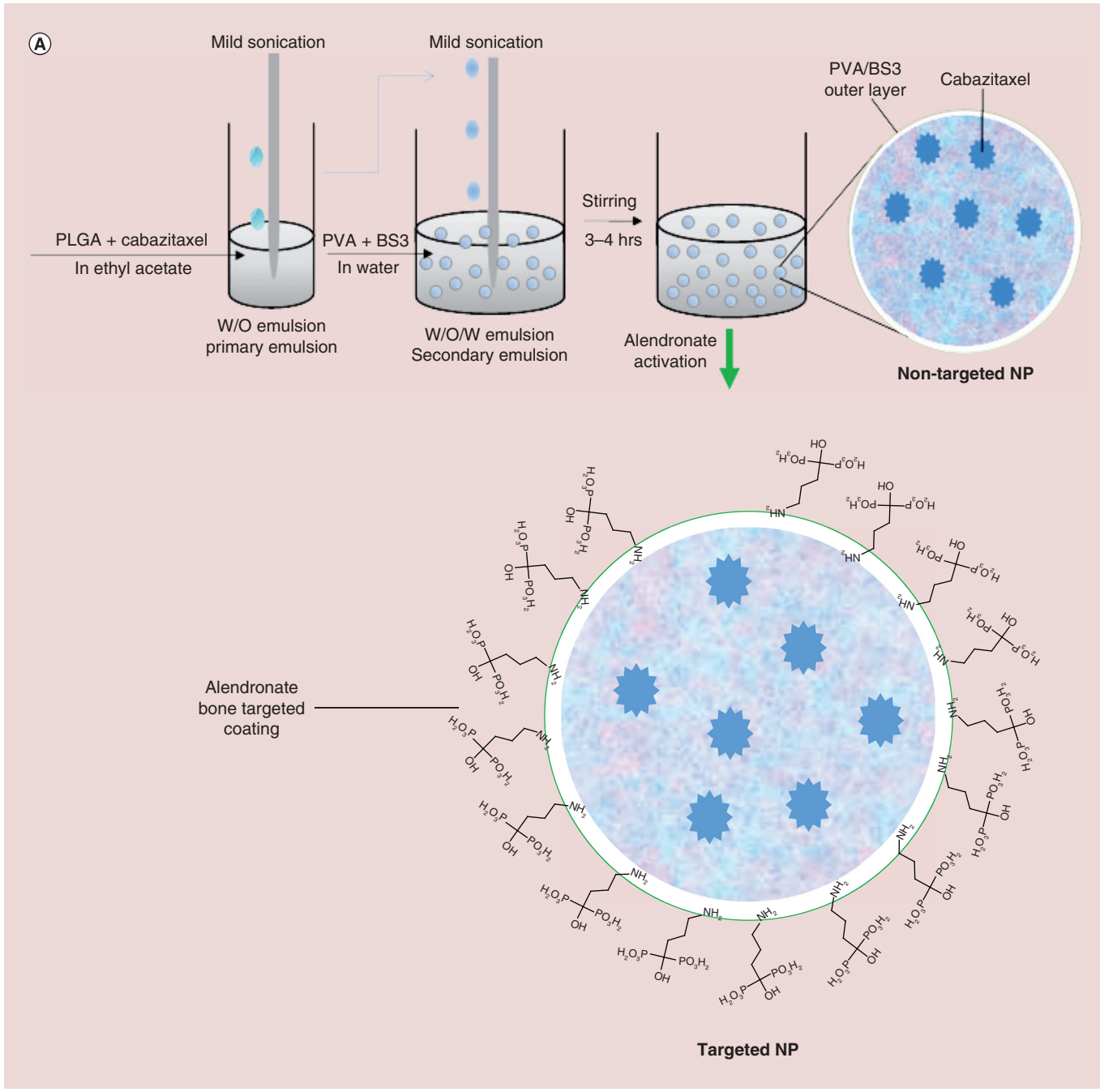

Figure 1. Nanoparticle physical characterization (also see facing page). **(A)** Schematic illustrating nanoparticle (NP) synthesis through water-in-oil-in-water double emulsion solvent evaporation technique followed by activation of nanoparticle with alendronate for bone targeting. **(B)** Size (red) and polydispersity index (blue) of nontargeted NP versus targeted NP. Mean ± SEM (n = 3). **p-value < 0.005. **(C)** Mean encapsulation efficiency of drug within nanoparticle at various initial concentrations of cabazitaxel in the NP formulation as a percentage of total weight of polymer and drug. **(D)** Release kinetics of cabazitaxel from NP at time points (1, 5, 8, 12, 24, 72 h). (Inset) magnification of time points (1, 5, 8 h). Mean ± SEM (n = 3). **(e)** Scanning electron microscopy images of nontargeted NP and targeted NP.

Von frey

The paw withdrawal threshold in response to mechanical stimulation was measured by applying calibrated von Frey filaments from underneath the cage through openings in the mesh floor to the hind paws. Mice were placed in separate transparent plexiglass chambers with a wire mesh floor underneath and acclimated to the test chamber for 2 min. A filament with 4.17 g of force was applied vertically to the plantar surface of the hind paw repeatedly ten-times with 10 s rest in between so the fil-

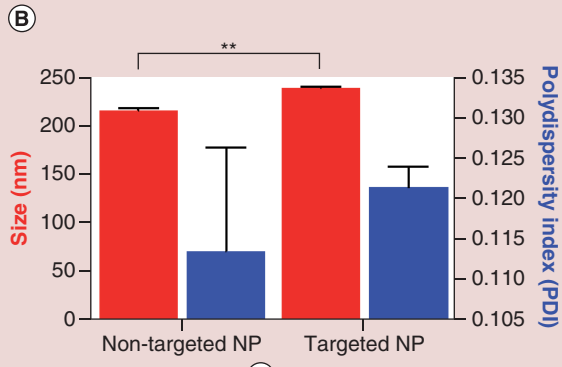

C

Initial cabazitaxel in NP formulation %	Encapsulation efficiency (%)	Drug loading (%)
0.5	37.7	0.3
1.0	27.9	0.4
2.0	45.5	1.1
3.0	48.8	1.6
4.0	55.3	2.5
5.0	55.8	3.7

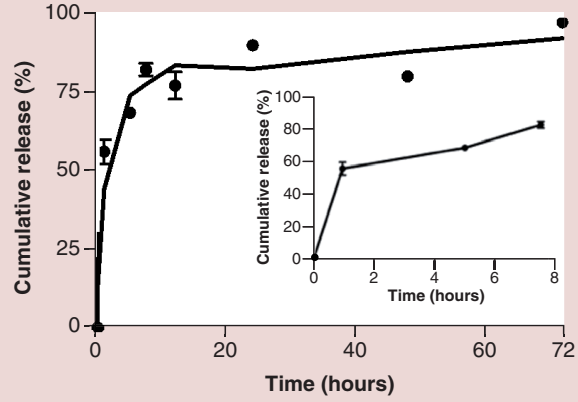

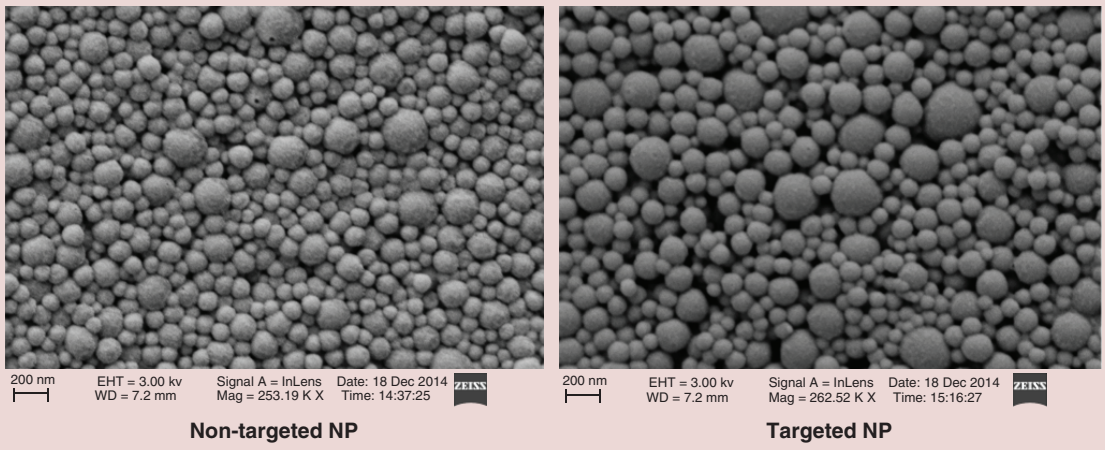

ament was bent during each test. The von Frey filament was chosen based on preliminary tests that showed to be intermediate between the lowest force with no response and the force which had consistent response. Brisk withdrawal, paw flinching or licking was considered a positive response and recorded. Both the right and left paw were measured. The response rate on the right where the tumor was implanted was subtracted from that of the left to control for inter-mouse variability.

Gait analysis

Gait was assessed with a simple footprint test. The hind paws were painted and the mouse was pretrained to walk in a straight line (two trials) over absorbent paper in a rectangular acrylic box made to mimic a dark alley lined with absorbent paper. The footprint patterns were analyzed for stride length and base width. Mice were assessed at three sessions each 1 week apart.

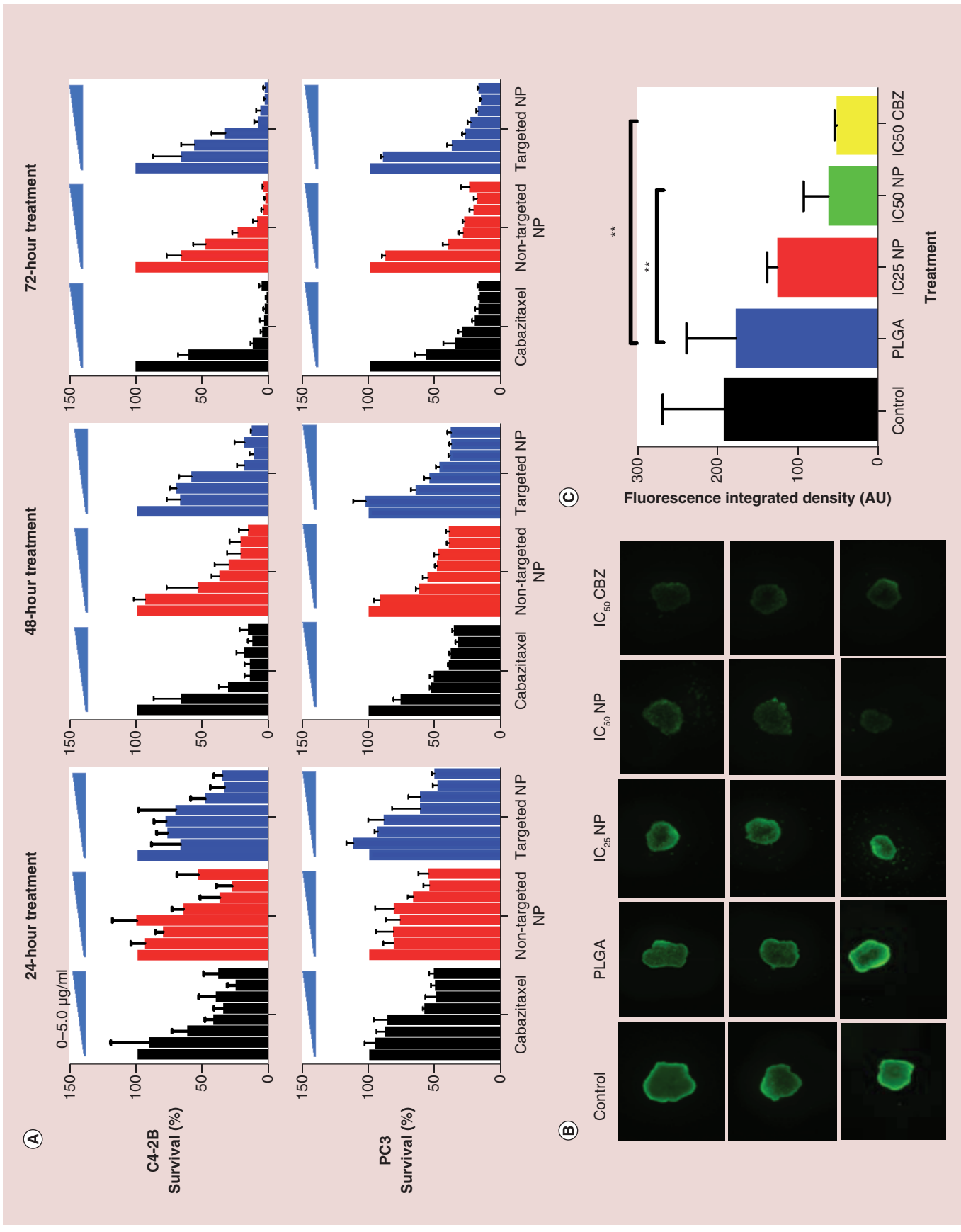
A
24-hour treatment
48-hour treatment
72-hour treatment
0–5.0 µg/ml
C4-2B Survival (%)
PC3 Survival (%)
150
100
50
0
Cabazitaxel
Non-targeted NP
Targeted NP
B
Control
PLGA
IC25 NP
IC50 NP
IC50 CBZ
C
Fluorescence integrated density (AU)
300
200
100
0
**
**
Control
PLGA
IC25 NP
IC50 NP
IC50 CBZ
Treatment

Figure 2. Nanoparticle *in vitro* studies (see facing page). (A) Dose and time dependent MTT growth inhibition assay of treatments in C4–2B (top row) and PC3 (bottom row) cell lines. Each cell line was treated for 24, 48 or 72 h with either cabazitaxel (black), nontargeted NP (red), or targeted NP (blue) at increasing concentrations (0.0000, 0.0005, 0.0050, 0.0100, 0.0250, 0.0500, 0.5000, 5.0000 μg/ml). Mean ± SEM (n = 3). **(B)** 3D Tumor Spheroid viability assay. Representative prostate spheroids were treated for 72 h with either DMSO as control vehicle (control), blank PLGA NP (PLGA), IC_{25} of cabazitaxel loaded Targeted NP (IC_{25} NP), IC_{50} of cabazitaxel (CBZ) loaded Targeted NP (IC_{50} NP), or the equivalent drug concentration of free cabazitaxel (IC_{50} Cab). After 72 h, spheroids were treated with calcein AM to determine spheroid viability. **(C)** Fluorescent integrated density quantification of prostate spheroids. Mean ± SEM (n = 4).
**p < 0.005.

Results

Formulation & physicochemical properties of nanoparticles

Nanoparticles were successfully synthesized by a double emulsion solvent evaporation technique in which cabazitaxel was encapsulated inside the nanoparticles and alendronate (ALN) was attached to the outside of the nanoparticles. Nanoparticles with alendronate decoration will be referred to as targeted NP. Nanoparticles that have no alendronate (prepared similar to targeted NP except the linkers neutralized with Tris buffer incubation) will be referred to as nontargeted NP. The optimal drug concentration was decided at 5% cabazitaxel to PLGA (w/w). This starting concentration yielded an encapsulation efficiency of 55.87% and drug loading of 3.74% (Figure 1). Thus, for all further experiments 5% was used as the drug to polymer ratio for formulating the NPs. Next, the hydrodynamic diameter of the nontargeted NP (Mean = 214.2 ± SD 2.27) and the targeted NP (Mean = 236.8 ± SD 1.19) was measured by dynamic light scattering. The polydispersity was also calculated for the nontargeted NP (Mean = 0.114 ± SEM 0.012) and the targeted NP (Mean = 0.121 ± SEM 0.003) (Figure 1B). Nanoparticles were imaged with scanning electron microscopy and shown to be of spherical shape with textured surface details as seen in (Figure 1E & F). No significant morphological differences were noted between the targeted and nontargeted NP.

The release kinetics of cabazitaxel from the nanoparticle were investigated *in vitro*. The cabazitaxel exhibited a strong initial burst phase release for 7.5 h with approximately 80% of the cabazitaxel being released from the nanoparticle during this time. This initial period was followed by a longer sustained release of the remaining cabazitaxel up to 98% cumulative drug released at 72 h (Figure 1D).

Nanoparticles are effective *in vitro* against prostate cancer cells

In 2D cellular viability assays (MTT assay), our results indicated that C4–2B cells were more sensitive to the treatments (free cabazitaxel, the nontargeted NP and the targeted NP) as compared with PC-3 cells. Additionally, the nanoparticle formulations compared with the free drug exhibited similar cell viability in the assays. No significant differences were observed between the nontargeted NP and the targeted NP groups. This was expected because the targeted mechanism is against the bone and not against the cancer cell *per se* and thus the targeting is not being tested in this assay. Finally, all treatment groups in both cell lines exhibited decreased survival at the longer treatment time points (Figure 2).

C4–2B cells were used to construct 3D spheroids as an *in vitro* model of prostate cancer. After treatment exposure, calcein AM was added to spheroids and fluorescence integrated density was used to quantify the difference in viability between treatment groups. Consistent with the results from the 2D cell viability assay, there was not a significant difference between spheroids treated with free drug and those treated with the equivalent dose of targeted NP. This suggests the possibility that the targeted NP provides comparable tumor inhibition through penetration of tumor spheroids. Additionally, the targeted NP group with no cabazitaxel loaded in it had the same viability as the saline treatment (Control) spheroid group which demonstrates that the targeted-NP without the cabazitaxel does not have any impact on cell viability (Figure 2B & C).

Targeted NPs have bone affinity

We investigated whether the targeted NP had the ability to bind to bone *ex vivo* by performing a bone binding assay. This assay showed a nearly fourfold increase of targeted NP binding to bone compared with nontargeted NP at the 6-h time point. The difference in binding of the targeted NP to the nontargeted NP was also increased to approximately fivefold and eightfold in the subsequent 24 and 72 h, respectively (Figure 3A & B).

Targeted NPs are effective at reducing tumor burden & maintaining bone structure

To determine the antitumor efficacy of the targeted-NP we used an intraosseous model of prostate cancer. Male athymic mice were injected intratibially with PC-3-luciferase cells. Tumors were allowed to develop for 7 days. At 7 days, mice were randomized into treatment groups based on bioluminescence signal of the PC-3

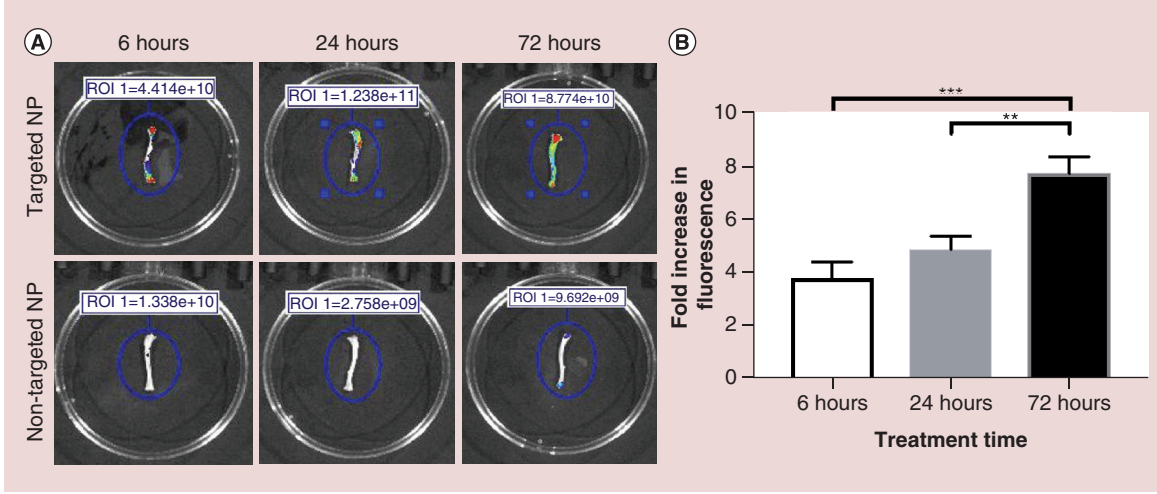

Figure 3. *Ex vivo* bone binding of nanoparticles. (A) Representative imaging with fluorescent overlay of mouse femurs after being incubated with either targeted nanoparticle (NP) tagged with fluorescent dye (top row) or nontargeted NP tagged with fluorescent dye (bottom row). Bones were incubated with NP for either 6, 24, or 72 h. **(B)** Quantification of fold increase in fluorescent signal between targeted NP and nontargeted NP at various time points. Mean ± SEM (n = 3).
**p < 0.005. ***p < 0.0005.

luciferase cells so that there was no statistically significant difference in starting tumor volume between groups. Mice were treated with intravenous injection weekly with one of the following treatments: Saline, cabazitaxel, nontargeted NP or targeted NP. After 1 month of treatment, mice were euthanized and lower limbs were isolated by excision at the knee and ankle joints and skin removal. Tumor burden was measured with bioluminescence signal as well as limb weight at termination of the experiment. When measuring tumor weight, both the targeted-NP and nontargeted NP groups showed a significant reduction in tumor compared with control treatment (p-value = 0.0001). The difference between the cabazitaxel group and the saline treated group was also significant but to a lesser degree (p-value = 0.002). When comparing the cabazitaxel treatment with the nanoparticle treatment groups, only the targeted NP treatment had a significant reduction in limb weight (p-value = 0.0447) (Figure 4D). When comparing the overall change in bioluminescence from the initial time point to the final week of the experiment, we observed a significant reduction in bioluminescence signal in the cabazitaxel group compared with the saline group (p-value = 0.0283) and an even more significant different between the targeted and the nontargeted NP group (p-values = 0.0027 and 0.0019, respectively) (Figure 4E).

We also investigated whether the targeted-NP impacts the physical structure of the bone through analysis of x-ray imaging in the tumor burdened limb prior to limb excision. Of note, we found that treatment with the targeted NP provided protection from bone lesions in all the mice imaged while those mice treated with the nontargeted NP showed bone lesions in 33% of the mice. Further, every mouse in the saline and cabazitaxel groups developed bone lesions (Figure 4C).

Targeted NPs improve pain response

To evaluate functional status, we assessed both pain via the von Frey assay and gait via paw print analysis. In the von Frey assay the targeted NP group significantly reduced the relative response to the filament in the tumor burdened limb (p-value = 0.026), whereas nontargeted NP and cabazitaxel treatments did not show a statistically significant relative reduction in response (Figure 5). Gait parameters that were measured included: stance width between opposite limbs, left limb stride distance and right limb stride distance. There were no significant differences between any treatment groups in gait parameters (results not shown).

Discussion

Our overall objective was to engineer an effective treatment for bone metastatic prostate cancer and test this therapy in a manner that can address some of the current challenges in treating bone metastatic prostate cancer. We have designed this targeted nanoparticle system with attention to addressing challenges at the molecular level, the tumor microenvironment and bone structure level, as well as the functional level.

Cabazitaxel was chosen as the cytotoxic agent for this nanoparticle system, which was successfully

loaded into the nanoparticle with an adequate encapsulation efficacy of 55.8% at a drug-polymer ratio of 5% (w/w) (Figure 1C). Cabazitaxel was chosen because it is a third generation microtubule inhibitor that was approved by the US FDA in 2010 for treating hormone-refractory metastatic prostate cancer that has progressed despite treatment with docetaxel. Unlike the older taxane drugs, paclitaxel and docetaxel,

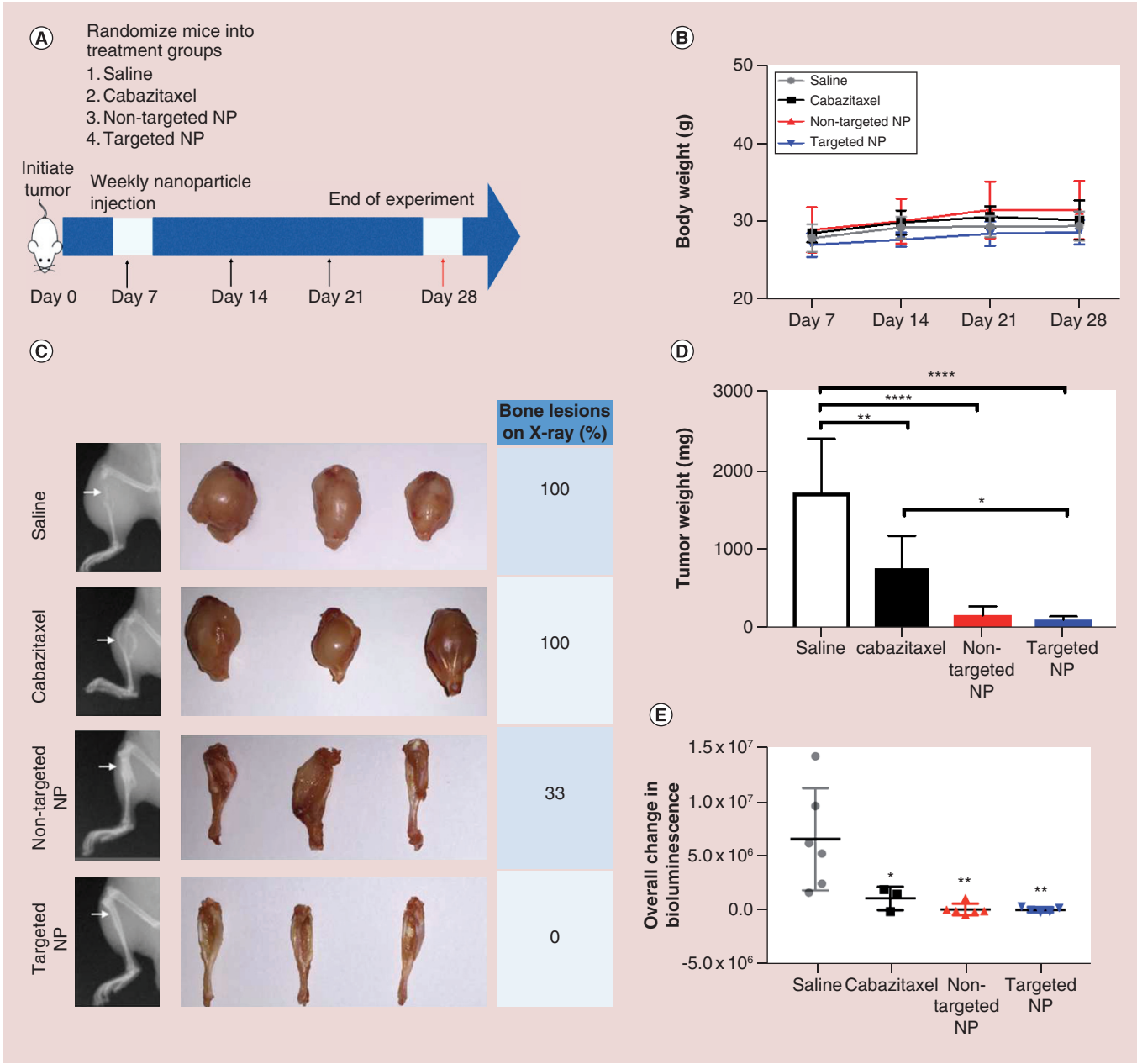

Figure 4. *In vivo* tumor efficacy study. (A) Schematic representing design of efficacy study. Tumors were initiated by injecting PC3 cells intraosseously in the tibia of mice. After 7 days mice were randomized into treatment groups based on bioluminescence signal to assure there were no significant differences in initial intraosseous tumor burden. Mice were injected via tail vein with either saline, cabazitaxel, nontargeted NP or targeted NP once every 7 days for 28 days. Mice were sacrificed at 28 days. **(B)** Mouse body weight measurement throughout experiment did not demonstrate a significant difference between treatments **(C)** (Middle) Representative images of excised tumors at the end of experiment. (Left) Representative x-ray images of mice bone structure at the end of experiment. Arrow shows tibia with bone lesion (saline, cabazitaxel, nontargeted NP) or intact bone (targeted NP). (Right) Percentage of mice in each group with bone lesions as measured by x-ray. **(D)** Final tumor weight of intratibial tumors after sacrifice. Mean ± SEM (n = 6 in all groups except targeted NP where n = 5). **(E)** Change in bioluminescence signal from day 7 to day 28. Mean ± SEM (n = 6 in saline and nontargeted groups, n = 5 in targeted NP, n = 3 for cabazitaxel group). ****p < 0.0001, **p < 0.005, *p < 0.05 using Dunnett's multiple comparisons test.

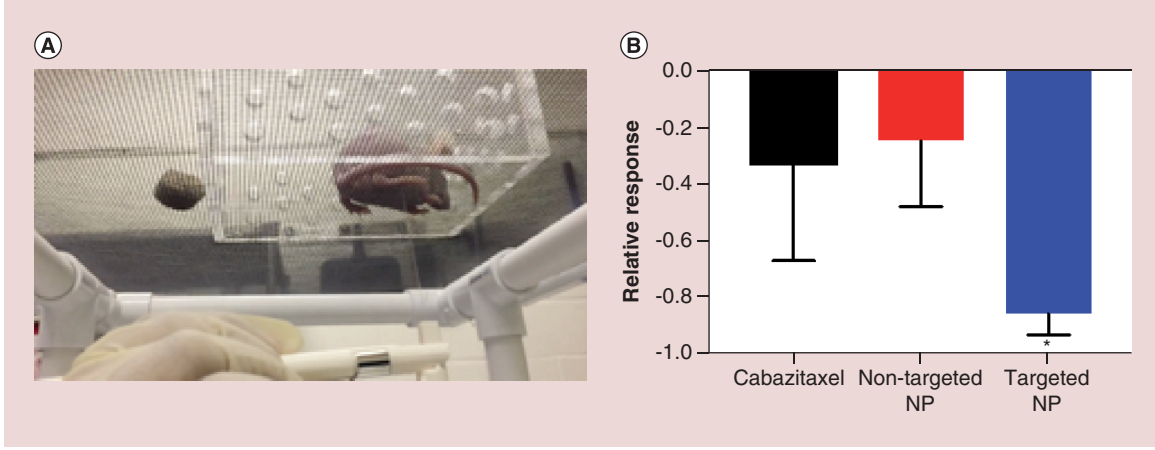

Figure 5. Animal behavioral von Frey monofilament assay. **(A)** Representation of experimental setup (video demonstration in supplemental. When mouse feels painful filament stimulus, it will lift limb in response). **(B)** Relative response of treatment groups as normalized to saline treatment group response (n = 6). There was a significant decrease in relative response to stimulus between saline and targeted NP groups when the untransformed data of saline and targeted NP were compared using ANOVA. Mean ± SEM (n = 6 in nontargeted NP group, n = 5 in saline and targeted groups, n = 2 in cabazitaxel group).
*$p < 0.05$.

cabazitaxel exhibits much lower substrate affinity for the ATP-dependent drug efflux pump glycoprotein (P-gp) that is commonly upregulated in metastatic and chemotherapy resistant cancers [14,15]. However, cabazitaxel does exhibit some toxicities that include: neuropathies, myelosuppression, febrile neutropenia, diarrhea, fatigue and asthenia among others [16]. The goal of formulating cabazitaxel in a targeted NP is to reduce the dosage of cabazitaxel and hence reduce its associated side effects.

There is a disparity in the literature as to the size nanoparticles should be made in order to provide best delivery to the tumor but most reports agree that a size less than 200–250 nm range is optimal [12]. We have manufactured the nanoparticles for this project to be within this size range with mean size of 236 nm after coating with alendronate (Figure 1B). Nanoparticles in this range can utilize passive targeting through the enhanced permeability and retention phenomenon while achieving active targeting with the alendronate coating.

In the *in vitro* cell viability studies, we found that addition of the targeting component, alendronate, to the targeted NPs did not increase growth inhibition in either the C4–2B or PC3 cell line. This was expected and similar results were seen in the 3D spheroid experiments, likely because of two reasons: the targeting mechanism of the alendronate moiety is against the hydroxyapatite structure of the bone and thus in this assay the targeting is not being tested and the alendronate does not have any intrinsic cytotoxic activity against cancer cells. The benefit of utilizing alendronate as a targeting component is realized in further studies where bone is introduced into the experimental models.

Our previous publications describe the linker system used to attach amine containing ligands, in this case ALN, to the nanoparticle surface [11,17]. This method noncovalently incorporates Bis[sulfosuccinimidyl] suberate (BS3) linker with its amine reactive N-hydroxysulfosuccinimide ester into a nanoparticle stabilizer coating consisting of poly(vinyl alcohol). The amine reactivity of the BS3 linker allows the amine group of ALN to be conjugated to the surface of the nanoparticle while the bisphosphonate groups of ALN are left reactive and facing outward with the ability to bind to hydroxyapatite. Bisphosphonates are used clinically as antiresorptive drugs that have high binding affinity for hydroxyapatite [18]. They are approved for use in a variety of conditions ranging from osteoporosis, multiple myeloma and Paget's disease, to palliation for various skeletally metastasized cancers. Additionally, because of its high osteotropism and known toxicity profile, our group as well as others have pursued various strategies to utilize bisphosphonates groups in conjugation to proteins, liposomes and nanoparticles so that therapeutics can be targeted to the bone [19–21]. However, cabazitaxel has not been utilized as a therapeutic payload in this context and few preclinical studies have investigated whether these bone targeted nanoparticle systems are effective in improving functional status and maintaining bone structure in the setting of bone metastatic cancer.

Using an intraosseous model of bone metastatic prostate cancer, we measured tumor burden using two orthogonal approaches, with limb tumor weights and

bioluminescence imaging. We found that all three treatment groups had a significant difference in tumor limb weight after the experiment and the nontargeted NP and targeted NP treatments had a very significant reduction in tumor size compared with the control group ($p = 0.0001$). Results of the bioluminescence imaging were consistent with the tumor weight studies. In addition, there was a significant difference between the targeted NP and free cabazitaxel treatment groups tumor limb weight ($p = 0.0447$), however no significant difference between the nontargeted and the free cabazitaxel groups (Figure 4). We speculate that the beneficial effect of both the targeted NP and nontargeted NP groups could be explained from the nature of a two-stage targeting effect. The first stage, utilizing the enhanced permeability and retention of the tumors by employing the size of the nanoparticle to concentrate the drug at the site of the tumor is used by both the targeted and nontargeted NP. While the second stage incorporates bone targeting by utilizing the alendronate coating on the surface of the targeted NP to bind the hydroxyapatite structure and further increase cabazitaxel at the lesion.

In addition to evaluation of tumor size, x-ray imaging revealed no bone lesions in the animals treated with targeted NPs. This is compared with the other treatment groups which developed varying degrees of lesions attributed to the osteoclastic nature of the lesions characteristic of the PC-3 cell line (Figure 4). We suspect that improved drug delivery to the lesion with the targeted NP served to mitigate bone damage by inhibiting the vicious cycle of bone destruction that occurs in the bone microenvironment setting.

Most literature evaluating preclinical therapeutic agents for bone metastatic cancer focus on tumor efficacy while neglecting an important clinical aspect, which is pain and functional status. In addition to studying the tumor efficacy *in vivo*, we have utilized animal behavioral assays in the overall evaluation of the bone targeted nanoparticles. Two behavioral assays were utilized to gauge whether the treatments had an impact on the functional status of the mice and the pain they experience. The first test was a gait analysis that can assess the change in gait pattern [22]. As the tumors and treatments progressed, a slight difference was observed in gait parameters measured in tumor burdened limb with a trend toward improved gait in the targeted NP group (data not shown). In addition, the von Frey assay was used to indicate functional pain status in these mice [23–25]. Interestingly, we found the group treated with targeted NPs had a significant reduction in relative response indicating they were experiencing less pain. These initial functional tests provide insight into the value of utilizing these targeted NP for bone metastatic prostate cancer and future research will focus on more functional status testing and elucidating more thoroughly the mechanisms involved.

Conclusion

This bone targeted nanoparticle system shows promise for treating bone metastatic prostate cancer. Notably, this targeted nanoparticle formulation showed efficacy in treating prostate cancer bone metastasis, improved bone structure and reduced pain from the bone tumor.

Summary points

Formulation & physicochemical properties of nanoparticles

- The amino-bisphosphate, alendronate, was conjugated to the surface of the nanoparticle (NP) to serve as a targeting moiety to the hydroxyapatite structure of the bone.
- Cabazitaxel was used as the cytotoxic agent against the prostate cancer cells and effectively encapsulated within the bone targeted nanoparticles.

Nanoparticles are effective *in vitro* against prostate cancer cells

- As expected, cell viability assays showed the targeted nanoparticles and the nontargeted nanoparticles to be as effective as the free drug in both 2D and 3D prostate cancer models.

Targeted NPs have bone affinity

- The phosphonate groups oriented on the exterior of the nanoparticle allow strong binding affinity for the hydroxyapatite structure of the bone.

Targeted NPs are effective at reducing tumor burden & maintaining bone structure

- Mice treated with bone microenvironment targeted nanoparticles had less tumor burden and improved quality of bone after 4 weeks of weekly intravenous tail vein treatments in an intraosseous model of bone metastasis.

Targeted NPs improve pain response

- Targeted nanoparticle therapy resulted in a reduction in pain as measured through von Frey filament assay.

Conclusion

- These results taken together show that this novel formulation of cabazitaxel bone microenvironment targeted nanoparticle not only reduces tumor volume but also maintains bone structure and diminishes pain experienced by mice with metastatic prostate cancer.

Financial & competing interests disclosure

This work was supported by grant awards from National Institutes of Health number R21CA194295 (to JK Vishwanatha) and 1P20 MD006882 (JK Vishwanatha), and the American Medical Association (A Gdowski) and the American Urological Association (A Gdowski). The authors have no other relevant affiliations or financial involvement with any organization or entity with a financial interest in or financial conflict with the subject matter or materials discussed in the manuscript apart from those disclosed.

No writing assistance was utilized in the production of this manuscript.

Ethical conduct of research

All animal studies were performed after approval from the Institutional and Animal Care and Use Committee.

Open access

This work is licensed under the Attribution-NonCommercial-NoDerivatives 4.0 Unported License. To view a copy of this license, visit http://creativecommons.org/licenses/by-nc-nd/4.0/

References

Papers of special note have been highlighted as: • of interest; •• of considerable interest

1 Coleman RE. Clinical features of metastatic bone disease and risk of skeletal morbidity. *Clin. Cancer Res.* 12(20 Pt 2), s6243–s6249 (2006).

2 Howlader NNA, Krapcho M, Miller D *et al. SEER Cancer Statistics Review, 1975–2013*. National Cancer Institute, MD, USA (2016).

3 Gartrell BA, Saad F. Managing bone metastases and reducing skeletal related events in prostate cancer. *Nat. Rev. Clin. Oncol.* 11(6), 335–345 (2014).

• **Provides a clinic overview of the managing bone metastatic prostate cancer.**

4 Saad F, Gleason DM, Murray R *et al.* A randomized, placebo-controlled trial of zoledronic acid in patients with hormone-refractory metastatic prostate carcinoma. *J. Natl Cancer Inst.* 94(19), 1458–1468 (2002).

5 Fizazi K, Carducci M, Smith M *et al.* Denosumab versus zoledronic acid for treatment of bone metastases in men with castration-resistant prostate cancer: a randomised, double-blind study. *Lancet* 377(9768), 813–822 (2011).

6 Petrylak DP, Tangen CM, Hussain MH *et al.* Docetaxel and estramustine compared with mitoxantrone and prednisone for advanced refractory prostate cancer. *N. Engl. J. Med.* 351(15), 1513–1520 (2004).

7 Tucci M, Bertaglia V, Vignani F *et al.* Addition of docetaxel to androgen deprivation therapy for patients with hormone-sensitive metastatic prostate cancer: a systematic review and meta-analysis. *Eur. Urol.* 69(4), 563–573 (2016).

8 Parker C, Nilsson S, Heinrich D *et al.* Alpha emitter radium-223 and survival in metastatic prostate cancer. *N. Engl. J. Med.* 369(3), 213–223 (2013).

• **Provides one of the first bone targeted agents that improves overall survival in the context of bone metastatic prostate cancer.**

9 Dansereau RN. A unique drug distribution process for radium Ra 223 dichloride injection and its implication for product quality, patient privacy, and delineation of professional responsibilities. *Ann. Pharmacother.* 48(11), 1512–1514 (2014).

10 Autio KA, Scher HI, Morris MJ. Therapeutic strategies for bone metastases and their clinical sequelae in prostate cancer. *Curr. Treat. Options Oncol.* 13(2), 174–188 (2012).

11 Thamake SI, Raut SL, Gryczynski Z, Ranjan AP, Vishwanatha JK. Alendronate coated poly-lactic-co-glycolic acid (PLGA) nanoparticles for active targeting of metastatic breast cancer. *Biomaterials* 33(29), 7164–7173 (2012).

• **This article was part of our previous work with bone targeting in metastatic breast cancer.**

12 Mohan S, Baylink DJ. Bone growth factors. *Clin. Orthop. Relat. Res.* (263), 30–48 (1991).

13 Wang F, Chen L, Zhang R, Chen Z, Zhu L. RGD peptide conjugated liposomal drug delivery system for enhance therapeutic efficacy in treating bone metastasis from prostate cancer. *J. Control. Release* 196, 222–233 (2014).

•• **Provides an excellent design and characterization of bone targeted liposomes and includes a reduction in pain as well as efficacy against the tumor.**

14 Paller CJ, Antonarakis ES. Cabazitaxel: a novel second-line treatment for metastatic castration-resistant prostate cancer. *Drug Des. Devel. Ther.* 5, 117–124 (2011).

15 Galsky MD, Dritselis A, Kirkpatrick P, Oh WK. Cabazitaxel. *Nat. Rev. Drug Discov.* 9(9), 677–678 (2010).

16 Nightingale G, Ryu J. Cabazitaxel (jevtana): a novel agent for metastatic castration-resistant prostate cancer. *PT* 37(8), 440 (2012).

17 Thamake SI, Raut SL, Ranjan AP, Gryczynski Z, Vishwanatha JK. Surface functionalization of PLGA nanoparticles by non-covalent insertion of a homo-bifunctional spacer for active targeting in cancer therapy. *Nanotechnology* 22(3), 035101 (2011).

18 Reszka AA, Rodan GA. Bisphosphonate mechanism of action. *Curr. Rheumatol. Rep.* 5(1), 65–74 (2003).

19 Swami A, Reagan MR, Basto P *et al.* Engineered nanomedicine for myeloma and bone microenvironment targeting. *Proc. Natl Acad. Sci. USA* 111(28), 10287–10292 (2014).

• **Provides evidence for effectiveness of a bone targeted nanoparticle loaded with bortezomib in the context of multiple myeloma.**

20 Chang Q, Geng R, Wang S, Qu D, Kong X. DOPA-based paclitaxel-loaded liposomes with modifications of transferrin

and alendronate for bone and myeloma targeting. *Drug Deliv.* 23(9), 3629–3638 (2016).

21 Doschak MR, Kucharski CM, Wright JE, Zernicke RF, Uludag H. Improved bone delivery of osteoprotegerin by bisphosphonate conjugation in a rat model of osteoarthritis. *Mol. Pharm.* 6(2), 634–640 (2009).

22 Lakes EH, Allen KD. Gait analysis methods for rodent models of arthritic disorders: reviews and recommendations. *Osteoarthritis Cartilage* 24(11), 1837–1849 (2016).

23 Blackburn-Munro G. Pain-like behaviours in animals - how human are they? *Trends Pharmacol. Sci.* 25(6), 299–305 (2004).

24 Lariviere WR, Wilson SG, Laughlin TM *et al.* Heritability of nociception. III. Genetic relationships among commonly used assays of nociception and hypersensitivity. *Pain* 97(1–2), 75–86 (2002).

25 Mogil JS, Crager SE. What should we be measuring in behavioral studies of chronic pain in animals? *Pain* 112(1–2), 12–15 (2004).